Graphene exfoliation in the presence of semiconducting polymers for improved film homogeneity and electrical performances

Tim Leydecker, Matilde Eredia, Fabiola Liscio, Silvia Milita, Georgian Melinte, Ovidiu Ersen, Michael Sommer, Artur Ciesielski and Paolo Samorì*

Dr. T. Leydecker, M. Eredia, Dr. A. Ciesielski, Prof. P. Samorì
ISIS & icFRC Université de Strasbourg & CNRS 8 allée Gaspard Monge 67000, Strasbourg, France
E-mail: samori@unistra.fr

Dr. F. Liscio, Dr. S. Milita
Istituto per la Microelettronica e Microsistemi (IMM) − CNR, via Gobetti 101, 40129 Bologna, Italy

Prof. Dr. M. Sommer
Institut für Makromolekulare Chemie, Stefan-Meier-Straße 31, 79104 Freiburg, Germany
Present address: TU Chemnitz, Institut für Chemie, Strasse der Nationen 62, 09111 Chemnitz, Germany

Dr. G. Melinte, Prof. O. Ersen
Institut de Physique et Chimie des Matériaux de Strasbourg (IPCMS), UMR 7504 CNRS – Université de Strasbourg, 23 rue du Loess, BP 43, 67034 Strasbourg cedex 2, France

Keywords: Graphene composites, Liquid phase exfoliation, Hybrid films, Organic semiconductors

*Corresponding author. Tel: +33 (0)3 68 85 51 60. E-mail: samori@unistra.fr (Paolo Samorì)
T. Leydecker and M. Eredia contributed equally to this work.

Abstract

We report on the production of hybrid graphene/semiconducting polymer films in one step procedure by making use of ultrasound-assisted liquid-phase exfoliation of graphite powder in the presence of π-conjugated polymers, i.e. poly(3-hexylthiophene) (P3HT) or poly[4-(4,4-dihexadecyl-4H-cyclopenta[1,2-b:5,4-b']dithiophen-2-yl)-alt-[1,2,5]thiadiazolo-[3,4-c]pyridine] (PCDTPT). The polymers were chosen in view of their different propensity to form crystalline structures, their decoration with alkyl chains that are known to possess high affinity for the basal plane of graphene, the energy levels of their frontier orbitals which are extremely similar to the work function of graphene, and their high electrical performance when integrated in field-effect transistors (FETs). The polymers act as a dispersion-stabilizing agent and prevent the re-aggregation of the exfoliated graphene flakes, ultimately enabling the production of homogeneous bi-component dispersions. The electrical characterization of few-layer graphene/PCDTPT hybrids, when integrated as active layer in bottom-contact bottom-gate FETs, revealed an increase of the field-effect mobility compared to the π-conjugated-based pristine devices, a result which can be attributed to the joint effect of the few-layer graphene sheets and semiconducting polymers improving the charge-transport in the channel of the field-effect transistor. In particular, few-layer graphene/PCDTPT films displayed a 30-fold increase of PCDTPT's mobility if compared to pristine polymer samples. Such findings represent a step forward towards the optimization of graphene exfoliation and processing into electronic devices, as well as towards improved electrical performance in organic-based field-effect transistors.

Graphene is a unique material holding outstanding physical properties,[1-4] which makes it interesting for a plethora of technological applications, e.g. in medicine,[5-7] flexible electronics[3, 8] and photonics,[4, 9, 10]. Such unique properties have been established on graphene produced by scotch tape or chemical vapour deposition (CVD), being both hardly up-scalable methods, thereby hampering any technological applications. Yet, graphene produced using milder and up-scalable strategies such as liquid-phase exfoliation, feature several drawbacks: (i) the yield of exfoliation, i.e. the amount of graphene that can be brought into a liquid media, is low, (ii) the electrical performance of the liquid-phase exfoliated graphene is modest, (iii) the deposition of the exfoliated graphene on surfaces into continuous monolayers is rather difficult.[11, 12] On the other hand, organic semiconductors (OSCs), while performing well but not flawlessly in terms of electrical performances (usually with a high I_{on}/I_{off} but modest mobility) have a different set of advantages, including the tunability of their physical properties *via* chemical functionalization,[13, 14] their reduced cost of processing[15, 16] in advantageous conditions (low temperature and ambient pressure), and their suitability for up-scalable processes even on flexible supports.[17] Graphene would benefit greatly from these characteristics, and because of this reason several attempts of combining these two types of materials have been reported in the literature.[18-25] These include multi-step procedures based on the subsequent deposition of a graphene and the polymeric semiconductor *via* spin-coating, ink-jet printing or thermal evaporation.[22, 23, 26] In particular, Torrisi and co-workers fabricated the active channel of a transistor by successive printing of graphene ink and poly[5,5′-bis(3-dodecyl-2-thienyl)-2,2′-bithiophene (PQT-12), reaching high electrical performances (mobility of 100 cm²/Vs).[26]

These approaches relied on the thermal annealing of the graphene film prior to the deposition of the OSC, being an effective strategy for the removal of the high boiling point solvent used for graphene exfoliation, and for fine-tuning of the graphene ionization energy before the OSC deposition by thermal annealing in air. However, they lack in terms of ease of

processing; moreover, the structural and electronic interactions between graphene and OSC is limited due to the face-to-face geometry of their interface, as the resulting active channel consists of two separate sandwiched layers. Aiming at achieving a greater electronic cross talk between the two components, previous attempts to hybrid organic/graphene film fabrication relied on blending graphene and OSCs in order to achieve higher performances.[18, 24, 25] In particular, it was recently demonstrated that liquid-phase exfoliated graphene can be co-deposited with a polymeric semiconductor and used in thin-film transistors in order to boost the ambipolar character of the polymer.[18] While this method is interesting, it does suffer from several drawbacks, including phase segregation between the two components,[18] graphene random aggregation,[19] crystallinity loss in the semiconductor matrix[20] and poor control over graphene deposition.[21]

One interesting approach could rely on the simultaneous blending of the OSCs with graphene during sonication-assisted exfoliation of graphite powder into graphene nanosheets, with OSCs acting as a dispersion stabilizing agents (DSAs) and preventing the re-aggregation of the exfoliated graphene flakes, ultimately enabling the production of homogeneous bi-component dispersions. This approach aims at exploiting the common strategy of adding DSAs to graphite dispersion before the exfoliation as a method for enhancing the exfoliation yield and stabilizing the graphene sheets in the solution.[27, 28] Moreover, unlike for the case of surfactants or small *ad hoc* molecules, polymers present in the dispersion will not need to be removed after the exfoliation, as they will be beneficial for charge transport properties of the hybrid material. For optimal performances, the most suitable polymer should be chosen in view of its structure, capacity to transport charges and energetic levels close to the work function of the graphene, i.e. around 5.0 eV.[18]

Here we show that the addition of the two *p*-type semiconductors, i.e. poly(3-hexylthiophene) (P3HT) or poly[4-(4,4-dihexadecyl-4H-cyclopenta[1,2-b:5,4-b']dithiophen-2-yl)-alt-[1,2,5]thiadiazolo-[3,4-c]pyridine] (PCDTPT) during the ultrasound-assisted liquid-phase

exfoliation process of graphite in *o*-DCB results in improved exfoliation towards the formation of a few-layer graphene (FLG). The electrical characterization of the resulting hybrid films revealed a strong improvement of electrical performances in the case of hybrid FLG/PCDTPT films compared to its pristine components.

We have focused our attention on P3HT and PCDTPT, two *p*-type OSCs (**Figure 1**). Both polymers possess similar HOMO level, 4.96 eV and 5.16 eV for P3HT and PCDTPT respectively (see **Table 1**), being close to the work function of graphene (4.94 eV, see **Figure S16**). Yet, these two polymers strongly differ in molecular arrangement in the solid state. The specific features of P3HT such as alkyl side chains and high molecular planarity enables its crystallization into domains possessing relatively high charge carrier mobilities[29], thereby making P3HT a prototypical *p*-type polymer semiconductor. For regioregular P3HT, the interplay of strong π- π stacking between adjacent core moieties and interdigitation of hexyl side chains belonging to neighbouring molecules favours the polymer-polymer interactions/stacking to form crystalline lamellae which may hinder the inter-mixing with graphene flakes. On the other hand, PCDTPT exhibits a limited planarity which determines a tendency to form amorphous structures both at the nano- and meso-scale. It features longer alkyl chains compared to P3HT, yielding a higher affinity for the basal plane of graphite/graphene[27, 30]. Moreover, the amorphous structure of PCDTPT and its rigid backbone is particularly well suited for intermixing with graphene nanosheets.

Few-Layer Graphene (FLG) and polymer composites were prepared by ultrasound-assisted liquid-phase exfoliation of synthetic graphite flakes[31] in 1,2-orthodichlorobenzene (*o*-DCB) in the presence of P3HT or PCDTPT. The choice of *o*-DCB is based on several criteria and the most important for our case study are: i) its surface tension of 36.6 mJ m^{-2} [32] makes it good candidate for the graphite exfoliation,[33] and ii) it is a good solvent for both P3HT[34] and PCDTPT.[35] Dispersions consisting of the polymers (5 mg/mL) and graphite powder (50 mg/mL) have been exposed for 6 hours to ultrasounds using a cup horn sonicator at a

frequency of 5 Hz (power of 50 W) in order to avoid both the degradation of the polymers and radical formation of the solvent molecules.[36] We have opted to use a high relative amount of graphite in order to produce high graphene-content films leading to a maximal impact of graphene in the electrical performances of the hybrid film. The electrical performances of the composites were studied by spin-coating dispersions of few-layer graphene/polymer as thin active films in the channel of a bottom-contact bottom-gate FETs with channel length L = 20 μm, supported on SiO_2. Since the aim of the study was not the optimization of the organic semiconductor performances through interface engineering, but rather the improvement of organic semiconductor performances through addition of few-layer graphene, pristine dielectric surface has been used without rendering it hydrophobic via octadecyltrichlorosilane (OTS) treatment. Moreover, *o*-DCB has been used as a solvent since it is compatible with graphene exfoliation processes and results in sub-par electrical performances. In order to evaluate the impact of graphene on the performance of OSC polymers a series of control experiments have been performed. In particular, control samples, i.e. mono-component films consisting of neat polymer (either P3HT or PCDTPT) and few-layer graphene (exfoliated in the absence of polymers), were prepared by spin-coating 150 μL solutions/dispersions in *o*-DCB at the concentration of 5 mg/mL and 50 mg/mL, respectively.

Figure 2a-f displays the morphology of these films as mapped by optical microscopy (OM) and atomic force microscopy (AFM). The obtained values of field-effect mobilities, I_{on}/I_{off} ratios and Root-Mean-Square Roughness (R_{RMS}) values are presented in **Table 2**. While the spin-coated films of both polymeric semiconductors exhibit smooth and homogeneous morphologies (R_{RMS} = 1-6 nm) as determined on AFM images sized 5*5 μm^2, the adsorption of graphene inks on solid substrates yields less homogeneous films featuring large aggregates that can reach tens of μm in lateral size (**Figure 2a**). The latter is in part due to the exfoliation process being performed by means of a cup horn sonicator. Such apparatus, when compared with the conventional ultrasonic baths, allows operating at low frequency, thereby avoiding

6

the extensive damaging of the materials during the exfoliation process, and it offers a more homogeneous ultrasound environment. Yet, the quality of the material exfoliated in the absence of OSCs is relatively poor as evidenced by the presence of aggregates of multi-layer graphene (MLG) and large un-exfoliated graphite particles observed by high-resolution transmission electron microscopy (HR-TEM) imaging as well (**Figures S1, S3**). The low quality of the films in terms of huge aggregates and inhomogeneous morphology can be ascribed also to other factors, including to the exfoliation carried out starting from a high concentration of graphite powder (50 mg/mL), the employed deposition method, i.e. spin-coating, and the modest interaction of the material with the SiO_2 substrate. **Figure 2g-i** report the electrical characterization performed on each type of mono-component film. FLG films exhibited its typical electrical characteristics lacking a semiconducting behaviour. Such a result can be ascribed to the presence of the graphite aggregates larger than the inter-electrodic channel and to the absence of bandgap in graphene. On the other hand, neat films of P3HT and PCDTPT revealed a semiconducting behaviour when spin-coated on a SiO_2 surface. In particular, the bottom-contact bottom-gate transistors exhibited p-type field-effect mobility around 10^{-2} and 4×10^{-3} cm²/Vs for P3HT and PCDTPT respectively and I_{on}/I_{off} exceeding 10^4 for both of them.

We have then focussed our attention to the electrical performance of the hybrid materials. 150 µL of each solution were spin-coated without additional purification steps or after filtering by using a filter with pore sizes of either 5 µm or 0.45 µm. AFM height images of the films and transfer curves of the characterized field-effect transistors are displayed in **Figure 3**. Noteworthy, typically the dispersions of single component 2D materials produced through liquid-phase exfoliation are not used directly, but only after purification or separation of the exfoliated flakes from the un-exfoliated material, e.g. by ultracentrifugation [37]. However, in the present case, single or multiple steps of centrifugation can lead to the occurrence of phase separation between graphene and conjugated polymers. To circumvent this problem, large

7

unexfoliated graphene aggregates have been removed by simple filtration of dispersions using polytetrafluoroethylene filters. A 5 μm filter was selected in order to keep in the dispersion only graphene flakes with a size just slightly smaller than the channel length (20 μm) (**Figure 3b,e**) while keeping the polymer "intact". The 0.45 μm filter was selected in order to retain in the dispersion only the smallest FLG flakes (**Figure 3c,f**) that may also act as small seed for the polymer crystallization. Films produced from filtered FLG dispersions (5 μm and 0.45 μm), i.e. exfoliated in the absence of the polymers, were also characterized by optical microscopy, AFM and by exploring their electrical properties (**Figure S1**). Optical microscopy and AFM show that only a low quantity of graphitic particles can be deposited by spin-coating after filtration, particularly in the case of 0.45 μm filter where neither film formation nor the presence of graphitic particles on SiO_2 substrate has been observed by optical microscopy (AFM image is not shown). Consequently, due to the absence of a continuous percolation path for the charges to move from the source to the drain electrode, any (semi-)conducting behaviour has been measured. This provides evidence for the difficulty of processing FLG solutions into homogeneous films.

In the case of the as-produced, i.e. unfiltered, few-layer graphene/P3HT solutions, the resulting films featured electrical characteristics which are similar to those of the graphene films, i.e. it does not exhibit any semiconducting behavior (**Figure 3g**). OM and AFM images confirm the assumption that graphene aggregates remain large enough to bridge the electrodes when the solution is not filtered (**Figure 3a,d**). However, an improvement in the homogeneity of the film is observed (R_{RMS} (graphene) = 14.5 nm; R_{RMS} (graphene:P3HT) = 13.4 nm, as determined on AFM images sized 3*3 $μm^2$), indicating that the bi-component approach to graphene deposition leads to a slightly more favorable deposition. Compared to the samples of neat FLG films, AFM characterization of material produced in the presence of P3HT (**Figure 3a,d**) showed the absence of large un-exfoliated flakes, which indicates clear improvement of the exfoliation. Together with fragmented graphite flakes, AFM imaging

shows the presence of flat and well-defined few-layered graphene flakes which, furthermore, offer a good coverage of the substrate thanks to the unifying presence of the polymer. Once filtered through 5 μm membrane, a very homogeneous film can be observed with a great amount of μm-sized multi-layer graphene flakes located all over the sample (**Figure 3b,e**). However, AFM height images evidenced the absence of thin flakes and mostly graphitic particles smaller than 1 μm are visible. Therefore, the electrical performances are not modified compared to a pristine P3HT film (mobility of 0.01 cm²/Vs, I_{on}/I_{off} of 10^5). Considering I_{on}/I_{off} close to 1 and the high off-current observed previously in the graphitic material (**Figure 2g**), the recovery of the electrical performances of P3HT (high I_{on}/I_{off}, low off-current, **Figures 2h** and **3h**), indicates the absence of a continuous pathway of graphitic material in the channel of the transistor. When the solution was filtered using a 0.45 μm filter, a very homogeneous film was produced (**Figure 3c**,**f**) but field-effect mobilities were lowered by a factor of 3 (**Figure 3i**; $\mu = 3 \times 10^{-3}$ cm²/Vs, I_{on}/I_{off} over 10^5).

Structural characterization of the films based on neat P3HT blended with graphite, was performed by X-ray diffraction in specular and grazing incidence geometries. They revealed that both the solution filtering and the graphite introduction affect the morphology and the polymer aggregation inside the film, i.e. the crystalline order and orientation. The specular scans are reported in **Figure 4a**; from the reflectivity (XRR) oscillations, observed in the region below q=0.2 Å^{-1}, morphological parameters of the films were extracted (see Table S2). The surface roughness drastically increases when P3HT is blended with FLG flakes (except for the blend obtained from a solution filtered by 0.45 μm pores) so that oscillations are damped and the numerical value cannot be extracted as observed by AFM images. Moreover, the film thickness remains constant, being ca. 13 nm.

In line with previous reports, P3HT aggregates in edge-on configuration on SiO$_2$ surface, as indicated by the presence of the lamellar peak (100) at q = 0.37 Å^{-1} in the specular scan (**Figure 4**), with spacing of 1.7 nm. Interestingly, the peak is clearly observed only for the un-

filtered P3HT. The vertical crystalline size extracted from the peak width matches with the film thickness, pointing that P3HT is well-stacked through the film. This is confirmed by the invariance of the reflection when the film is probed at different penetration depths (**Figure S4, S5**). The observation of multiple diffraction orders, i.e. (100), (200) and (300) reflections along the out-of-plane direction in the 2D GIWAXS images (**Figures S4, S5**), points out the high crystalline order typical for this polymer. The introduction of graphene in the blend affects the orientation of the polymer aggregation. Indeed, for un-filtered and 5 μm filtered solution, the lamellar peaks appear along the in-plane direction and decrease along the out-of-plane direction, indicating the addition of P3HT in face-on orientation (likely lying on graphene's surface).

Despite a change in morphology and in the orientation of the polymer aggregation, no change in electrical performances is observed (mobility of 0.01 cm²/Vs and I_{on}/I_{off} over 10^3 in both cases, **Table 2**). This could be due to the low amount of graphitic particles upon filtering (**Figure 3e**).

When using a 0.45 μm-size filter the polymer appears being amorphous, as proven by the almost disappearance of lamellar peaks (**Figure 4**, **S4**, **S6**), thereby explaining the lowering of the field-effect mobility

Films of graphite exfoliated in the presence of PCDTPT were produced and characterized following the same procedure with OM and AFM images as well as transfer curves, presented in **Figure 5**. Unlike pure FLG and P3HT based solutions, graphite exfoliated in the presence of PCDTPT leads to homogeneous films of PCDTPT with a high concentration of a few-layer graphene flakes without any large graphitic aggregates, as evidenced by both the optical and AFM images (**Figure 5a,d**). In addition, the transfer curves do not feature high I_{DS} current unaffected by V_{GS} (**Figure 5g**), unlike previously observed in the case of pure few-layer graphene (**Figure 2g**) and hybrid graphene/P3HT depositions (**Figure 3g**). This result is particularly remarkable since it indicates that PCDTPT promotes

the exfoliation of graphite into graphene, forming a well-intermixed bi-component material that can be processed into homogeneous films (R_{RMS} (graphene) = 14.5 nm and R_{RMS} (Graphene:PCDTPT) = 11.8 nm as determined on a 3*3 μm^2 and 2*2 μm^2 images, respectively). The molecular structure of PCDTPT can explain the difference in exfoliation as it is a more rigid and planar polymer compared to P3HT. Furthermore, the recorded transfer curves did not display the typical behavior of films containing big graphitic particles bridging the electrodes. On the contrary, the resulting transfer curve (**Figure 5g**) is an addition of current issued from graphitic material and the tested polymer, implying that both materials play an important role in the charge carrier transport between the source and drain electrodes. The measured field-effect mobility of the hybrid films exceeded 0.1 cm²/Vs, being 30-fold greater than pure PCDTPT films. This is due to charges travelling through both materials, leading to charge transport characteristics that combine those intrinsic to both materials. The addition of FLG leads to an increase of both the mobility and the I_{off} current, as compared to pristine PCDTPT. In order to explain this result, the effect of the addition of graphite before exfoliation was investigated by means of X-ray diffraction in specular and grazing incidence geometries.

From XRR (**Figure 6a**) oscillations analysis, the surface roughness results to be almost the same for all the films, except for the blend obtained from an unfiltered solution. In this case, the high roughness is due to the presence of thick FLG sheets.

For $q > 0.2$ Å^{-1}, the specular scan of 20 nm thick PDCTPT film (**Figure 6a**) displays the (100) peaks hinting a lamellar structure, with spacing 2.6 nm, when the film is prepared from an unfiltered solution. GIWAXS images collected on the same film (**Figures S10**, **S11**) show typical features of a polymer aggregation with edge-on orientation where (100) and (010) reflections, the latter coming from the π-π stacking periodicity, appear along the out-of-plane and in-plane directions, respectively. The polymer aggregation is homogenous along the film thickness, as evidenced by the persistence of Bragg reflections, although weak due to the low

crystalline order, on GIWAXS images collected at different penetration depths (see **Figure S11**).

As observed for P3HT, since the film thickness does not change when the solution is prepared from filtered solution (**Table S2**), the absence of Bragg reflections on both specular scan and GIWAXS images (**Figure 6**, **S10**, **S12**) suggests that small aggregates are already formed in solution and successively transferred to the substrate surface. It could be that the filter removes the aggregates (e.g. resulting from the self-aggregation of the longest polymers) and consequently the polymer self-organizes in amorphous phase once deposited on the surface.

With the introduction of few-layer graphene, the (100) and (200) lamellar peaks along the specular direction (**Figure 6**, **S10**, **S12**, **S13**) broadens, whereas they appear narrower along the in-plane direction, indicating the interaction between PDCTPT and graphene surface induces the polymer to self-organize in a face-on configuration. The film is therefore composed of two different populations of aggregates: one with edge-on configuration on silicon oxide and the other face-on on graphene surfaces.

Hence, the XRD data is perfectly coherent with the electrical characterization. While the I_{on} is mostly, yet not exclusively, dependent on the layer of semiconductor at the interface with the dielectric, the I_{off} is mostly dependent on the bulk of the semiconducting film. The observed transfer curve is therefore a combination of charge transport at the interface (PCDTPT aggregated in edge-on configuration, high I_{on}/I_{off}, low current) and charge transport in the bulk (PCDTPT aggregated in face-on configuration on graphene, high I_{on} and I_{off} currents).

The filtering of the solutions with 5 μm-sized pores did only evidence a minor change in the global electrical performances within the obtained devices due to the reduced roughness. AFM images seem to indicate a lower concentration of FLG after filtering of the solution using a 5 μm pore size filter. While in the case of exfoliation in the presence of P3HT, FLG was removed upon filtration (**Figure 5e**), films produced from the filtered PCDTPT solution still contained some FLG, demonstrating a stronger interaction of graphene with the polymer

12

(**Figure 5e**). A small reduction in the mobility is measured, combined with a large decrease of the conductivity due to the reduced amount of graphitic material within the film. Films produced from a solution filtered using a 0.45 μm-sized pores lead to the presence of very few small graphitic aggregates within a layer of PCDTPT. Bragg peaks disappear when the 0.45 μm-sized filter is used, confirming that the polymer already aggregates in solution.

In summary, we have demonstrated a straightforward one-step procedure in which hybrid graphene-based composites are prepared via sonication-assisted liquid-phase exfoliation of graphite in the presence of suitably selected π-conjugated polymers. Even as very mild sonication parameters were used for the exfoliation, strong interactions between graphitic material and the organic semiconductors P3HT and PCDTPT were observed. GIWAXS data provided evidence that FLG exfoliated in the presence of PCDTPT exhibits to good coverage once spin-coated, with homogeneous polymer aggregation along the film thickness.

The selection of an adequate polymer is the key parameter for achieving high electrical performances, as demonstrated by blends of graphite and PCDTPT that resulted in a 30-fold improvement of the mobility upon exfoliation and spin-coating. These performances were obtained from unfiltered solutions, highlighting the role of aggregation at the solution stage of fabrication. Furthermore, investigation of the differences in aggregation between bulk and semiconductor/dielectric interface lead to better understanding of the electrical characteristics measured in hybrid FLG/polymer films. These findings represent a gateway towards the optimization of graphene exfoliation, deposition and performance increase, as they highlight the importance of the selection of an adequate polymer (with energy level matching those of graphene and an ability to self-organize on graphene) added before the exfoliation of 2D-materials and the effect of FLG/polymer aggregation on electrical performances.
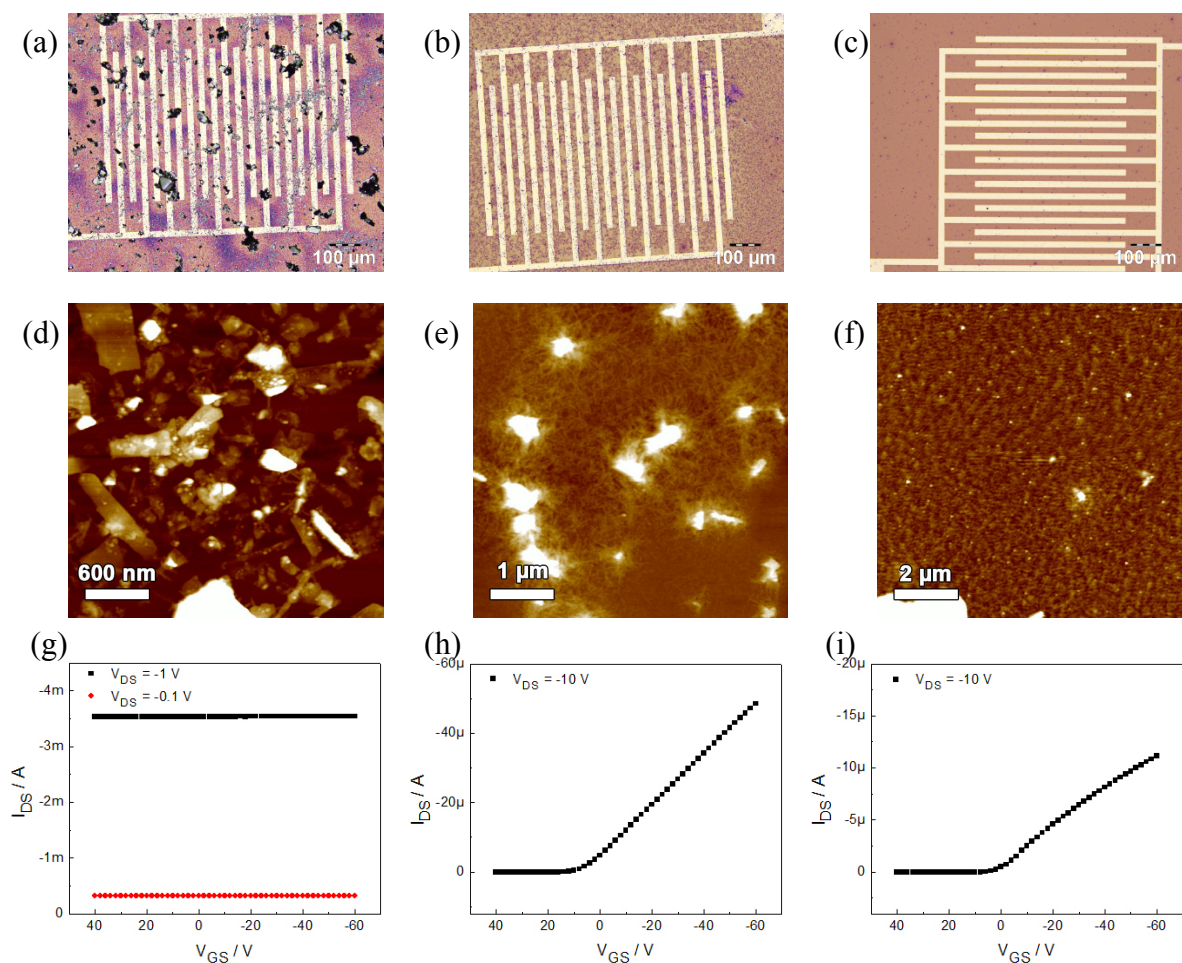
13
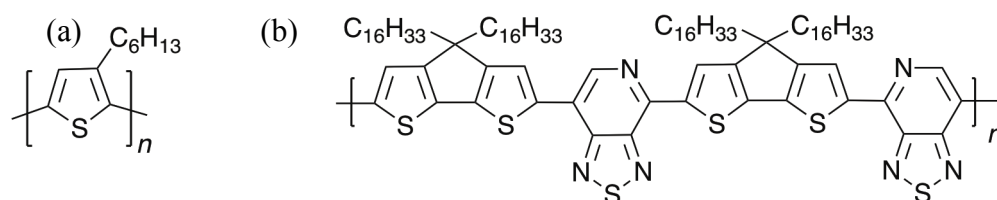
Figure 1. Chemical structure of the two chosen *p*-type polymeric semiconductors: (a) P3HT, and (b) PCDTPT.
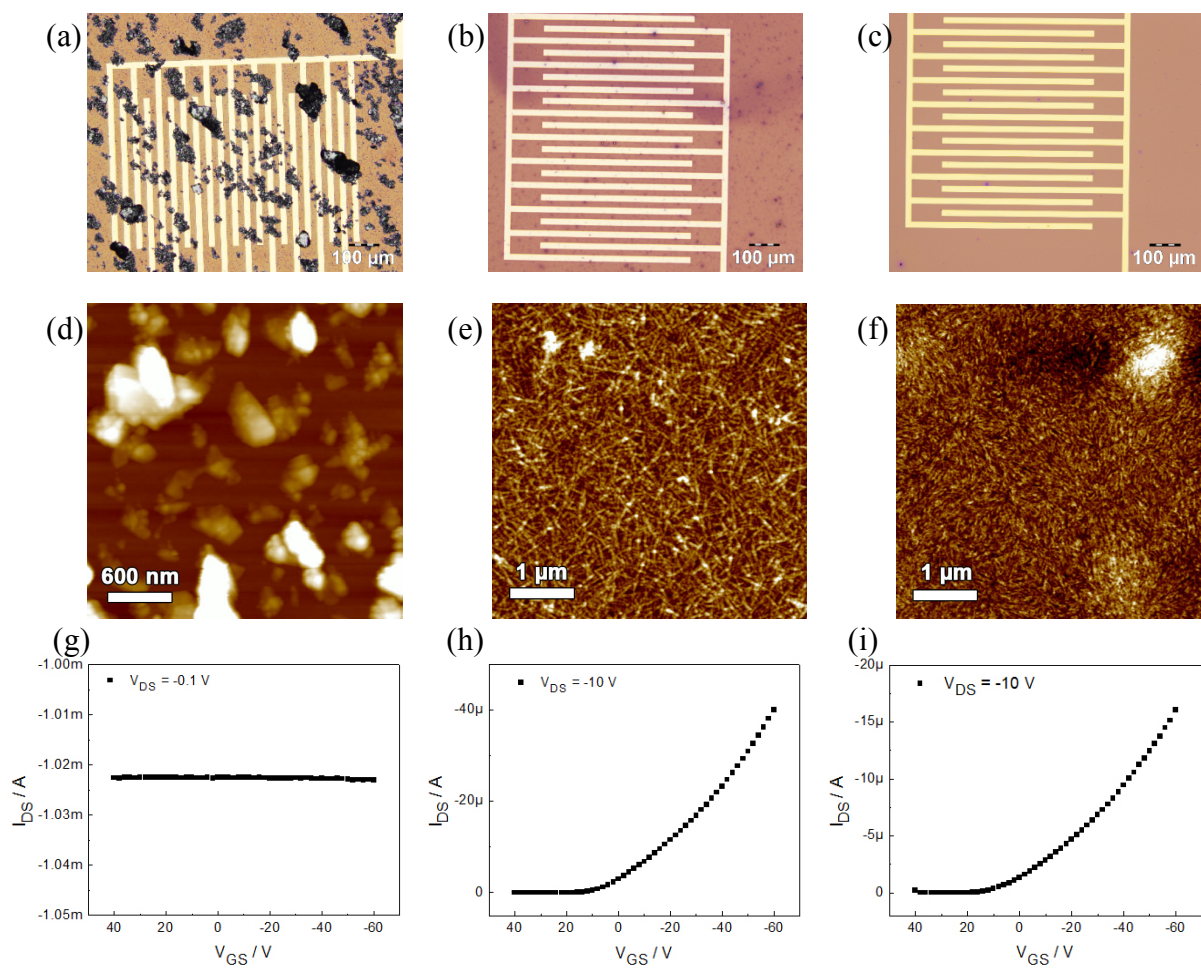
Figure 2. OM, topographical AFM and transfer curves of films produced from (a,d,g) dispersions of neat graphitic material exfoliated in 1,2-dichlorobenzene, (b,e,h) solutions of pure P3HT [L = 20 µm, V_{DS} = -0.1 V], and (c,f,i) solutions of pure PCDTPT. Z-scales: (d) 72 nm; (e) 48 nm; (f) 8 nm.
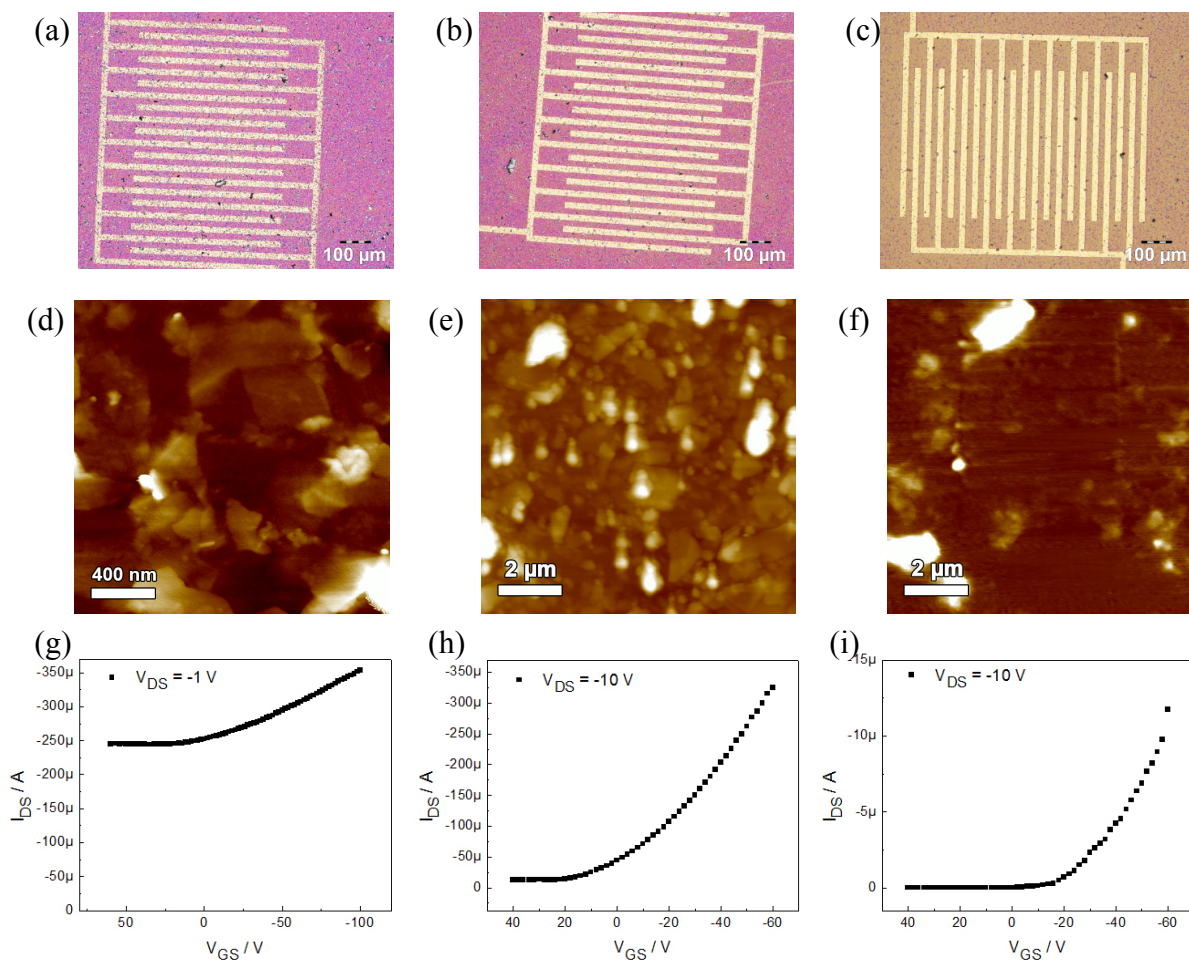
Figure 3. OM, topographical AFM and transfer curves of films produced from dispersions of graphite exfoliated in the presence of P3HT. (a,d,g) pristine solution, as well as after filtering using a pore-sized filter: (b,e,h) 5 μm, and (c,f,i) 0.45 μm. Z-scales: (d) 55 nm, (e) 78 nm, (f) 20 nm.
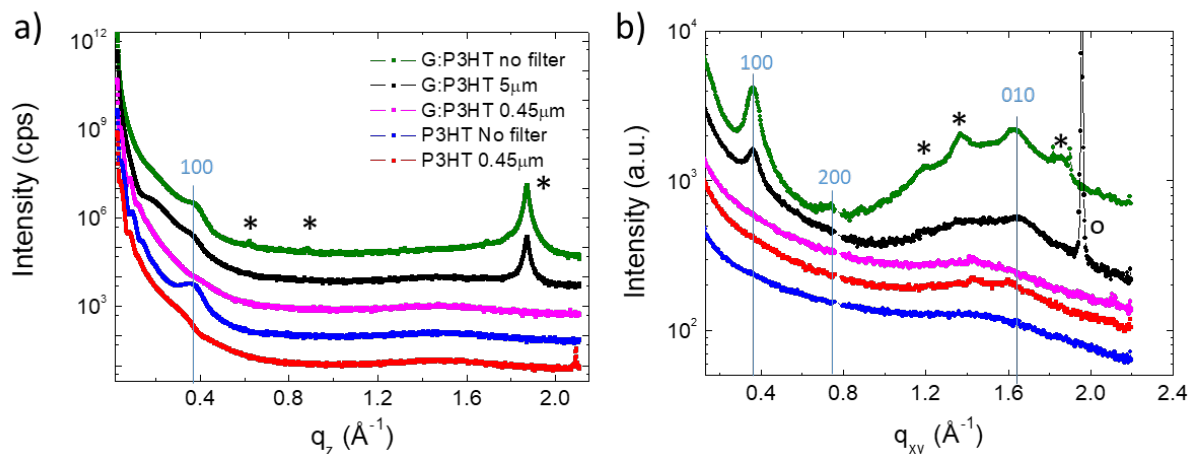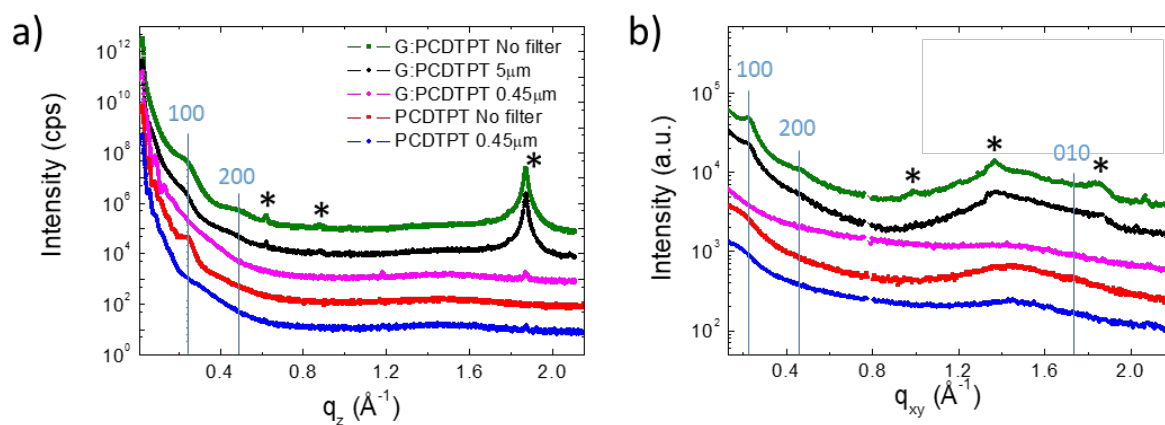

Figure 4. (a) Specular scans, and (b) in-plane integrated intensities of GIWAXS images (**Figure S4**) of the P3HT and few-layer graphene:P3HT spin-coated films, shifted for clarity.

Bragg peaks coming from graphene solution and substrate are labelled by stars and open circles, respectively.

Figure 5. OM, topographical AFM and transfer curves of films produced from dispersions of graphitic material exfoliated in the presence of PCDTPT. (a,d,g) pristine solution, as well as after filtering using a pore size of (b,e,h) 5 µm, and (c,f,i) 0.45 µm. Z-scales: (d) 86 nm; (e) 358 nm, (f) 77 nm.

Figure 6. (a)Specular scans and (b) in-plane integrated intensities of GIWAXS images (**Figure S10**) of the PCDTPT and FLG:PCDTPT spin-coated films, shifted for clarity. Bragg peaks coming from graphene solution are labelled by stars.

Table 1. HOMO and LUMO energy levels of the conjugated polymers P3HT and PCDTPT.

Material	HOMO [eV]	LUMO [eV]	Band gap [eV]
P3HT[38]	-4.96	-3.04	1.92
PCDTPT[39]	-5.16	-3.70	1.46

All reported values for polymers were obtained from cyclic voltammetry in the cited works. The work function of the FLG, measured by Ambient Photoelectron Spectroscopy (see supporting information, **Figure S15**), amounted to -4.94 eV.

Table 2. Summary of the electrical performances and Root-Mean-Square Roughness (R_{RMS}) of the pristine and hybrid films.

Material	Filter pore size	μ / cm²/Vs	I_{on}/I_{off}	R_{RMS} / nm
FLG	/	/	1	14.5
P3HT	/	1×10^{-2}	10^5	5.87
PCDTPT	/	4.2×10^{-3}	10^6	1.05
FLG:P3HT	/	/	1	13.4
FLG:P3HT	5 µm	1×10^{-2}	10^5	11.2
FLG:P3HT	0.45 µm	3×10^{-3}	10^6	1.3
FLG:PCDTPT	/	1.2×10^{-1}	1.4	11.8
FLG:PCDTPT	5 µm	8×10^{-2}	30	43.2
FLG:PCDTPT	0.45 µm	5×10^{-3}	10^6	12.8

All reported values were obtained from the transfer curves presented in **Figures 1**, **2** and **4**.

References

[1] A.K. Geim, K.S. Novoselov, The rise of graphene, Nat. Mater. 6(3) (2007) 183-191.
[2] K.S. Novoselov, A.K. Geim, S.V. Morozov, D. Jiang, Y. Zhang, S.V. Dubonos, et al., Electric field effect in atomically thin carbon films, Science 306(5696) (2004) 666-669.
[3] A.C. Ferrari, F. Bonaccorso, V. Fal'ko, K.S. Novoselov, S. Roche, P. Boggild, et al., Science and technology roadmap for graphene, related two-dimensional crystals, and hybrid systems, Nanoscale 7(11) (2015) 4598-4810.
[4] F. Bonaccorso, Z. Sun, T. Hasan, A.C. Ferrari, Graphene photonics and optoelectronics, Nature Photon. 4(9) (2010) 611-622.
[5] G. Lalwani, A.M. Henslee, B. Farshid, L.J. Lin, F.K. Kasper, Y.X. Qin, et al., Two-Dimensional Nanostructure-Reinforced Biodegradable Polymeric Nanocomposites for Bone Tissue Engineering, Biomacromolecules 14(3) (2013) 900-909.
[6] W.R. Yang, K.R. Ratinac, S.P. Ringer, P. Thordarson, J.J. Gooding, F. Braet, Carbon Nanomaterials in Biosensors: Should You Use Nanotubes or Graphene?, Angew. Chem. Int. Edit. 49(12) (2010) 2114-2138.
[7] R. Kurapati, K. Kostarelos, M. Prato, A. Bianco, Biomedical Uses for 2D Materials Beyond Graphene: Current Advances and Challenges Ahead, Adv. Mater. 28(29) (2016) 6052-6074.
[8] S. Bae, H. Kim, Y. Lee, X.F. Xu, J.S. Park, Y. Zheng, et al., Roll-to-roll production of 30-inch graphene films for transparent electrodes, Nat. Nanotechnol. 5(8) (2010) 574-578.
[9] J.D. Roy-Mayhew, I.A. Aksay, Graphene Materials and Their Use in Dye-Sensitized Solar Cells, Chem. Rev. 114(12) (2014) 6323-6348.

[10] J.B. Wu, M. Agrawal, H.A. Becerril, Z.N. Bao, Z.F. Liu, Y.S. Chen, et al., Organic Light-Emitting Diodes on Solution-Processed Graphene Transparent Electrodes, Acs Nano 4(1) (2010) 43-48.

[11] D.A. Boyd, W.H. Lin, C.C. Hsu, M.L. Teague, C.C. Chen, Y.Y. Lo, et al., Single-step deposition of high-mobility graphene at reduced temperatures, Nat. Commun. 6 (2015).

[12] F. Schwierz, Graphene transistors, Nat. Nanotechnol. 5(7) (2010) 487-496.

[13] Y.C. Mei, M.A. Loth, M. Payne, W.M. Zhang, J. Smith, C.S. Day, et al., High Mobility Field-Effect Transistors with Versatile Processing from a Small-Molecule Organic Semiconductor, Adv. Mater. 25(31) (2013) 4352-4357.

[14] R. Nouchi, Y. Kubozono, Anomalous hysteresis in organic field-effect transistors with SAM-modified electrodes: Structural switching of SAMs by electric field, Org. Electron. 11(6) (2010) 1025-1030.

[15] H. Yan, Z.H. Chen, Y. Zheng, C. Newman, J.R. Quinn, F. Dötz, et al., A high-mobility electron-transporting polymer for printed transistors, Nature 457(7230) (2009) 679-U1.

[16] S.R. Forrest, Exciton formation statistics under electrical injection in organic semiconductor thin films, J. Lumin. 110(4) (2004) 378-383.

[17] A.C. Arias, J.D. MacKenzie, I. McCulloch, J. Rivnay, A. Salleo, Materials and Applications for Large Area Electronics: Solution-Based Approaches, Chem. Rev. 110(1) (2010) 3-24.

[18] M. El Gemayel, S. Haar, F. Liscio, A. Schlierf, G. Melinte, S. Milita, et al., Leveraging the Ambipolar Transport in Polymeric Field-Effect Transistors via Blending with Liquid-Phase Exfoliated Graphene, Adv. Mater. 26(28) (2014) 4814-4819.

[19] S. Basu, F. Adriyanto, Y.H. Wang, Blending effect of 6,13-bis (triisopropylsilylethynyl) pentacene-graphene composite layers for flexible thin film transistors with a polymer gate dielectric, Nanotechnology 25(8) (2014).

[20] J. Huang, D.R. Hines, B.J. Jung, M.S. Bronsgeest, A. Tunnell, V. Ballarotto, et al., Polymeric semiconductor/graphene hybrid field-effect transistors, Org. Electron. 12(9) (2011) 1471-1476.

[21] A. Kumari, I. Singh, N. Prasad, S.K. Dixit, P.K. Rao, P.K. Bhatnagar, et al., Improving the efficiency of a poly(3-hexylthiophene)-CuInS2 photovoltaic device by incorporating graphene nanopowder, J. Nanophotonics 8(1) (2014) 083092.

[22] T. Mosciatti, S. Haar, F. Liscio, A. Ciesielski, E. Orgiu, P. Samorì, A Multifunctional Polymer-Graphene Thin-Film Transistor with Tunable Transport Regimes, Acs Nano 9(3) (2015) 2357-2367.

[23] T.J. Ha, D. Akinwande, A. Dodabalapur, Hybrid graphene/organic semiconductor field-effect transistors, Appl. Phys. Lett. 101(3) (2012).

[24] X. Huang, X.Y. Qi, F. Boey, H. Zhang, Graphene-based composites, Chem. Soc. Rev. 41(2) (2012) 666-686.

[25] R. Bkakri, O.E. Kusmartseva, F.V. Kusmartsev, M. Song, A. Bouazizi, Degree of phase separation effects on the charge transfer properties of P3HT:Graphene nanocomposites, J. Lumin. 161 (2015) 264-270.

[26] F. Torrisi, T. Hasan, W.P. Wu, Z.P. Sun, A. Lombardo, T.S. Kulmala, et al., Inkjet-Printed Graphene Electronics, Acs Nano 6(4) (2012) 2992-3006.

[27] A. Ciesielski, P. Samorì, Graphene via sonication assisted liquid-phase exfoliation, Chem. Soc. Rev. 43(1) (2014) 381-398.

[28] D. Li, M.B. Muller, S. Gilje, R.B. Kaner, G.G. Wallace, Processable aqueous dispersions of graphene nanosheets, Nat. Nanotechnol. 3(2) (2008) 101-105.

[29] R.P. Kurta, L. Grodd, E. Mikayelyan, O.Y. Gorobtsov, I.A. Zaluzhnyy, I. Fratoddi, et al., Local structure of semicrystalline P3HT films probed by nanofocused coherent X-rays, Phys. Chem. Chem. Phys. 17(11) (2015) 7404-7410.

[30] J.P. Rabe, S. Buchholz, Commensurability and Mobility in 2-Dimensional Molecular-Patterns on Graphite, Science 253(5018) (1991) 424-427.

[31] Y. Hernandez, V. Nicolosi, M. Lotya, F.M. Blighe, Z.Y. Sun, S. De, et al., High-yield production of graphene by liquid-phase exfoliation of graphite, Nat. Nanotechnol. 3(9) (2008) 563-568.

[32] C.E. Hamilton, J.R. Lomeda, Z.Z. Sun, J.M. Tour, A.R. Barron, High-Yield Organic Dispersions of Unfunctionalized Graphene, Nano Lett. 9(10) (2009) 3460-3462.

[33] S. Haar, A. Ciesielski, J. Clough, H.F. Yang, R. Mazzaro, F. Richard, et al., A Supramolecular Strategy to Leverage the Liquid-Phase Exfoliation of Graphene in the Presence of Surfactants: Unraveling the Role of the Length of Fatty Acids, Small 11(14) (2015) 1691-1702.

[34] J.Y. Na, B. Kang, D.H. Sin, K. Cho, Y.D. Park, Understanding Solidification of Polythiophene Thin Films during Spin-Coating: Effects of Spin-Coating Time and Processing Additives, Sci Rep-Uk 5 (2015).

[35] H.W. Luo, C.M. Yu, Z.T. Liu, G.X. Zhang, H. Geng, Y.P. Yi, et al., Remarkable enhancement of charge carrier mobility of conjugated polymer field-effect transistors upon incorporating an ionic additive, Sci Adv 2(5) (2016).

[36] A. Ciesielski, S. Haar, A. Aliprandi, M. El Garah, G. Tregnago, G.F. Cotella, et al., Modifying the Size of Ultrasound-Induced Liquid-Phase Exfoliated Graphene: From Nanosheets to Nanodots, Acs Nano 10(12) (2016) 10768-10777.

[37] F. Bonaccorso, A. Lombardo, T. Hasan, Z.P. Sun, L. Colombo, A.C. Ferrari, Production and processing of graphene and 2d crystals, Mater. Today 15(12) (2012) 564-589.

[38] E. Orgiu, N. Crivillers, J. Rotzler, M. Mayor, P. Samori, Tuning the charge injection of P3HT-based organic thin-film transistors through electrode functionalization with oligophenylene SAMs, J Mater Chem 20(48) (2010) 10798-10800.

[39] L. Ying, B.B.Y. Hsu, H.M. Zhan, G.C. Welch, P. Zalar, L.A. Perez, et al., Regioregular Pyridal[2,1,3]thiadiazole pi-Conjugated Copolymers, J. Am. Chem. Soc. 133(46) (2011) 18538-18541.